Chinese Chemical Letters 36 (2025) 110898

Contents lists available at ScienceDirect

Chinese Chemical Letters

journal homepage: www.elsevier.com/locate/cclet

Metal single-atom catalysts derived from silicon-based materials for advanced oxidation applications

Hanghang Zhao[a], Wenbo Qi[a], Xin Tan[c,*], Xing Xu[b], Fengmin Song[a], Xianzhao Shao[a,*]

[a] School of Chemical and Environment Science, Shaanxi University of Technology, Hanzhong 723001, China
[b] Shandong Key Laboratory of Water Pollution Control and Resource Reuse, School of Environmental Science and Engineering, Shandong University, Qingdao 266237, China
[c] Shandong Resources and Environment Construction Group Co., Ltd., Ji'nan 250100, China

ARTICLE INFO

Article history:
Received 8 November 2024
Revised 25 December 2024
Accepted 21 January 2025
Available online 21 January 2025

Keywords:
Advanced oxidation processes
Single-atom catalysts
Silicon
Fenton-like reaction
Degradation

ABSTRACT

Enhancing the corrosion resistance of carriers within Fenton-like systems and inhibiting the migration and aggregation of single atoms in reaction environments are essential for maintaining both high activity and stability at catalytic sites, thus meeting fundamental requirements for practical application. The Fenton-like process of activating various strong oxidants by silicon-based single atom catalysts (SACs) prepared based on silicon-based materials (mesoporous silica, silicon-based minerals, and organosilicon materials) has unique advantages such as structural stability (especially important under strong oxidation conditions) and environmental protection. In this paper, the preparation strategies for the silicon-based SACs were assessed first, and the structural characteristics of various silicon-based SACs are systematically discussed, their application process and mechanism in Fenton-like process to achieve water purification are investigated, and the progress of Fenton-like process in density functional theory (DFT) of silicon-based derived single atom catalysts is summarized. In this paper, the preparation strategies and applications of silicon-based derived SACs are analyzed in depth, and their oxidation activities and pathways to different pollutants in water are reviewed. In addition, this paper also summarizes the device design and application of silicon-based derived SACs, and prospects the future development of silicon-based SACs in Fenton-like applications.

1. Introduction

Metal single-atom catalysts (SACs) have garnered increasing attention in the field of catalysis due to their atomic dispersion of active sites and high catalytic activity [1–8]. Single-atom catalysis represents a novel research area within heterogeneous catalysis [3,9–13]. However, compared to vapor phase and electrochemical catalysis, aqueous single-atom catalysis remains relatively understudied, particularly in terms of its application in the catalytic oxidation of organic pollutants in water. Over recent decades, there has been significant interest from both scientific and industrial communities in developing remediation techniques for refractory organic pollutants, driven by increasingly stringent global environmental regulations and society's strong desire for a healthy environment [3,14–16]. The Fenton reaction is widely regarded as one of the most effective advanced oxidation processes (AOPs) for degrading organic pollutants by generating highly reactive hydroxyl radicals (•OH) through H_2O_2 activation. Although Fe^{2+} or Fe^{3+} homogeneous catalysts are commonly employed in Fenton or Fenton-like reactions, they suffer from issues such as iron leaching, sludge formation, recovery difficulties, and limited pH working range [17–23]. To address these challenges, heterogeneous Fenton oxidation has emerged as an alternative approach that utilizes supported iron catalysts; however, this comes at the expense of sacrificing the high activity observed with homogeneous catalysis. Nevertheless, supported metal catalysts still face limitations due to their inherent tendency towards metal site accumulation which results in a small number of exposed metal sites available for reaction. Maximizing the dispersion of active iron sites can enhance the activity of Fenton-like catalysis [11,24–27]. Single-atom catalysts have gained widespread use across various catalytic reactions owing to their potential to achieve atomic-level dispersion on support materials such as carbon nitride and graphene [3,28–31].

However, while pursuing the high catalytic activity of single atom catalysts, it is equally crucial to consider the continuity of their activated peroxides in Fenton-like systems and prioritize high

* Corresponding authors.
E-mail addresses: 15053106508@163.com (X. Tan), xianzhaoshao@snut.edu.cn (X. Shao).

https://doi.org/10.1016/j.cclet.2025.110898
1001-8417/

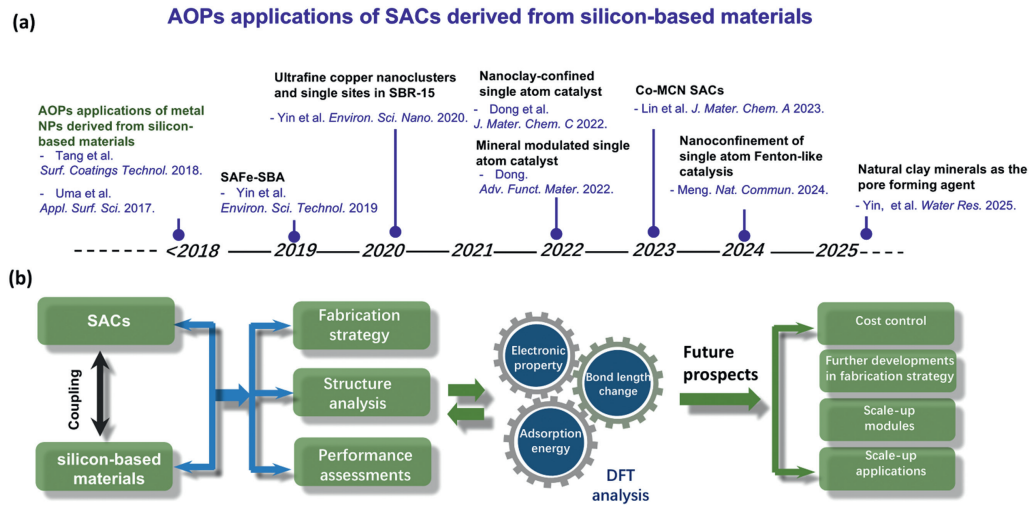

Fig. 1. (a) Timeline for the developments of metal single-atom catalysts derived from silicon-based materials for advanced oxidation applications. (b) Scheme flow of this review.

stability for practical applications [3,28–31]. Despite carbon-based SAC coordination structures exhibiting exceptional Fenton-like reactivity, numerous scholars have observed that carbon-based SACs are not highly recyclable, typically experiencing a reduction of nearly 10%−50% after four to six cycles [3]. This limitation poses a significant bottleneck in their practical application. One key reason is the susceptibility of carbon-based supports to severe corrosion under prolonged strong oxidation conditions, leading to the loss or agglomeration of single atom sites and resulting in a substantial decline in catalytic performance. Therefore, enhancing the corrosion resistance of SACs carriers within Fenton-like systems and inhibiting the migration and aggregation of single atoms under reaction environments are essential for maintaining both high activity and stability at catalytic sites, thus meeting fundamental requirements for practical applications [3]. Emerging research indicates that compared to carbon-based supports, silicon-based alternatives such as mesoporous silica, silicon-based minerals, and organosilicon materials exhibit superior oxidation resistance and corrosion resistance [5,32–37]. Consequently, they can serve as ideal carriers ensuring stability at single atom catalytic sites within robust Fenton-like oxidation systems.

In recent years (2019 to date), there has been a few amount of literature on the synthesis of silicon-based single-atom catalysts (SACs) from silicon-based materials [34]. Timeline for the developments of metal single-atom catalysts derived from silicon-based materials for advanced oxidation applications was shown in Fig. 1a. This review presents innovative methods for preparing silicon-based SACs, introduces their main structural catalytic mechanisms, analyzes their performance and mechanism in advanced oxidation applications, clarifies the catalytic mechanism of silicon elements combined with computational methods, analyzes the understanding of geometric and electronic characteristics of silicon-based SACs, and predicts key properties and reactivity. Scheme flow of this review was given in Fig. 1b. The review aims to provide a comprehensive understanding of the synthesis methods for SACs based on silicon and reveal reaction pathways in target catalysis processes. Finally, challenges related to designing silicon-based SACs are discussed along with prospects for cost-effective equipment in future research.

2. Fabrication of SACs derived from silicon-based materials

The main precursors for the preparation of silicon-based single atom catalysts encompass diverse silicon-based materials, such as mesoporous silica, silicon-based minerals, and organosilicon materials [5,32–37]. Among all these silicon-based materials, mesoporous silica is prevalently employed. Mesoporous silica is a material featuring a regular nano-scale pore structure, with its pore size ranging from 2 nm to 50 nm. This material possesses a high specific surface area, typically ranging from 500 m^2/g to 1500 m^2/g, high mechanical strength, and thermal stability, controllable synthesis, and adjustable pore size and specific surface area.

Li and co-workers developed a series of silica supported Co-SACs (CoNC-MSi) with tailored nanoconfined pore sizes (CoNC-MSi_1: 7.7 nm, CoNC-MSi_2: 12.8 nm) through a coupled impregnation-calcination method [5], as shown in Figs. 2a and b. After being highly dispersed in acetone, 2,3-dihydroxynaphthene and mesoporous silica were centrifuged, dried, and calcined in a nitrogen atmosphere to obtain mesoporous silica with a graphitic carbon coating [5]. Subsequently, $Co(OAC)_2{\cdot}4H_2O$ and 1,10-phenanthroline were introduced and calcined at 800 °C to yield CoNC-MSi catalyst. They discovered that the porous shell bestowed the CoNC-MSi with a 6.8-fold larger specific surface area than the nonporous sample, and the large surfaces of the nanoconfined catalysts provided abundant anchoring sites for Co single atoms (Fig. 2c). Aberration-corrected high-angle annular dark-field scanning (AC-HAADF-STEM) was an essential golden index for SAC detection, and the result also indicated that Co atoms were successfully loaded in the confined channel (Figs. 2d-f). In reality, most SACs derived from mesoporous silica were fabricated based on the template method, that is, an etching process using HF, NH_4HF_2, or NaOH was requisite for the removal of the silica-based template [33,36,38,39]. For example, Lin *et al.* fabricated a series of Co-SACs using mesoporous silica as the silica-based template [36]. The mesoporous silica microspheres with a size of approximately 300 nm were prepared by the Stober-like method. After nitrogen calcination at 520 °C, the gap of SiO_2 microspheres was filled with dicyandiamide//$Co(C_5H_7O_2)_2$, and then etched with NH_4HF_2 (Fig. 2g). The macroporous structure was formed in the as-prepared Co-SACs, with the uniform dispersion of atomic Co (0.6–10.2 wt%) being observed (Figs. 2h and i). They also reported that mesoporous silica as the template established strong metal-support interactions (MSIs) to stabilize and activate atomically dispersed Co species. Fundamentally, regardless of the etched or unetched mesoporous silica-based SACs, the stability of the support structure with mesoporous silica, coupled with the strong MSIs, could restrain the aggregation of metal single atoms, resulting in relatively stronger catalytic activity and durability [36].

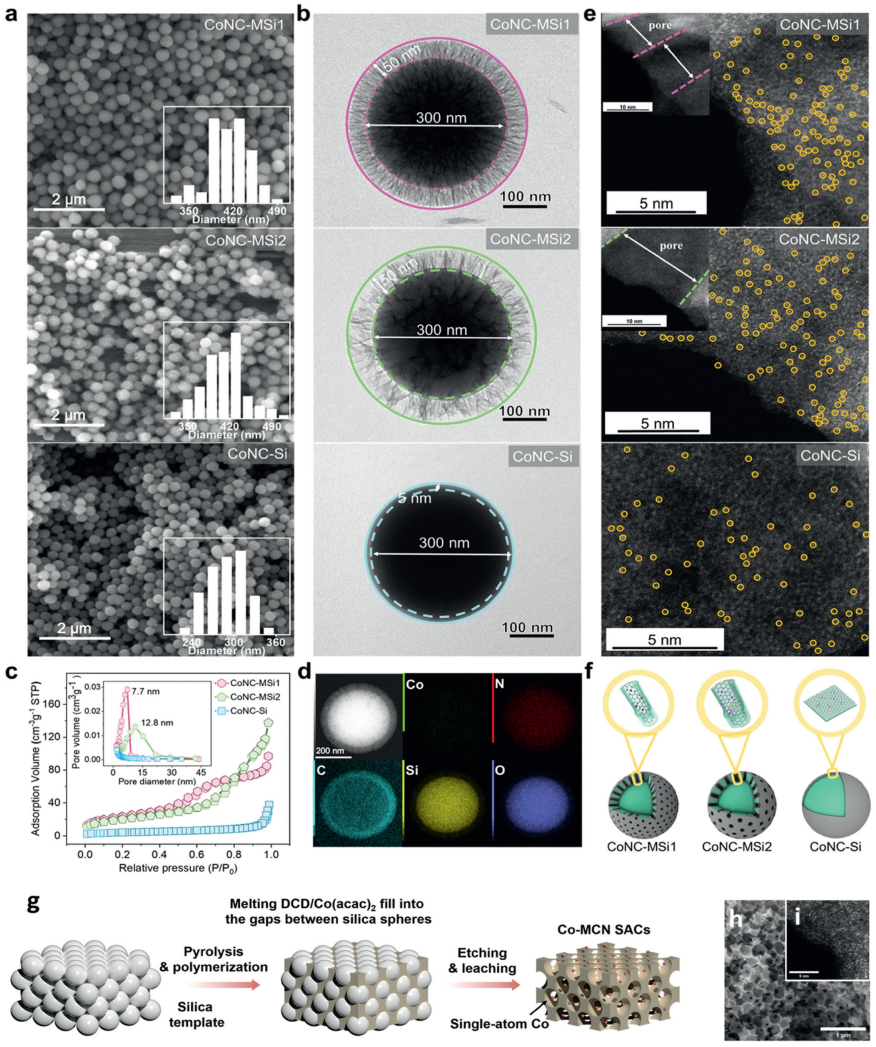

Fig. 2. (a) Scanning electron microscope (SEM) images of various CoNC-MSi catalysts and their particle size distributions. (b) Transmission electron microscope (TEM) images of various CoNC-MSi catalysts. (c) N_2 adsorption-desorption isotherms and the pore size distribution curves of various CoNC-MSi catalysts. (d) EDS mapping of CoNC-MSi1 catalyst. (e) AC-HAADF-STEM images of CoNC-MSi. (f) Schematic diagram of the catalyst spatial structure. Reproduced with permission [5]. Copyright 2024, The Nature Ltd. (g) Scheme of the silica template for preparation of Co-SACs. (h) SEM image of the Co-SACs. (i) AC-HAADF-STEM images of the Co-SACs. Reproduced with permission [36]. Copyright 2024, The Royal Society of Chemistry.

As a typical mesoporous silica, the SBA-15 has been intensively utilized as a support material in numerous applications, such as oxygen evolution reaction, gas adsorption, catalytic hydrogenation, and catalytic hydrogenation deoxidation, owing to its ordered nanopore structure, large specific surface area, and moderate pore size [12,34,35,40]. Sun and colleagues reported for the first time that the introduction of single-atom Fe sites in SBA-15 nanopores (SAFe-SBA) *via* straightforward strategy of directly loading Fe onto SBA-15 before roasting [34]. In this strategy, the iron precursor $Fe(NO_3)_3$ was thoroughly mixed with the as-prepared SBA-15 by solid-state grinding (Fig. 3a). During the subsequent calcination process, the conversion of $Fe(NO_3)_3$ and the removal of the template can be accomplished simultaneously. $Fe(NO_3)_3$ decomposes in the confined space with a large number of Si-OH groups, thereby enabling the iron site to be dispersed in the nanopore at the atomic level. The HAADF-STEM image of SAFe-SBA and corresponding element mapping revealed a mesoporous hexagonal array in the as-prepared catalyst and no nanoparticles can be observed in the HAADF-STEM image (Fig. 3b). Additionally, the element mapping indicated that the iron sites were uniformly dispersed in the nanopores (Figs. 3c and d), and no particle aggregation was observed in the nanopores. The XAFS results demonstrate that the four H atoms on the Si-OH surface are replaced by Fe atoms to form Fe-O bonds (Figs. 3e and f). The simulation results of four Fe-O bonds with an average of 1.81 Å are in accordance with the experimental data of the Fe coordination number 4.5 and the Fe-O bond length 1.89 Å (Fig. 3g). Similarly, Yin *et al.* employed P123/SBA-15 as a carrier, and ultrafine CuO nanoclusters and Cu single atoms could be anchored to the SBA-15 carrier [35]. The abundant silica hydroxyl group (Si-OH) and the restricted space in P123/SBA-15 ensured that the catalyst UNCu-SBA does not have copper site aggregation. By replacing the three H atoms of Si-OH, a single Cu atom is doped into SBA-15 to form three Cu-O bonds with an average bond length of 1.93 Å, which is consistent with the experimental data of 1.94 Å and the coordination number of a single Cu bond (Figs. 3h and i). Furthermore, some nanoclusters were identified in the mesoporous channels, which might be accountable for the lag ring delay in the N_2 adsorption isotherm mentioned above (Figs. 3j and k). Therefore, the ordered nanopore structure, large specific surface area, and moderate pore size of mesoporous silica provide a way for various methods/routines to anchor the metal single-atom sites within the mesoporous silica, which is the crucial reason why mesoporous silica is the predominant silicon-based SACs.

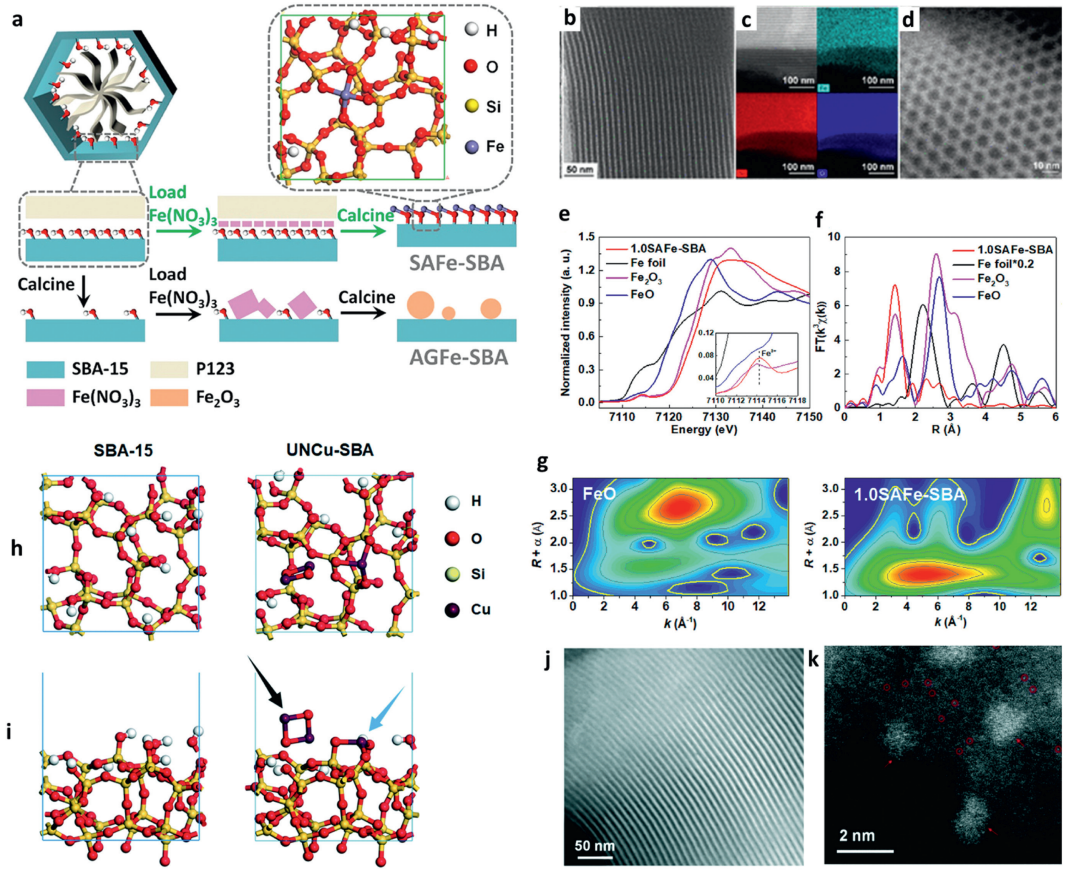

Fig. 3. (a) Introduction of single-atom Fe sites in SBA-15 nanopores for fabrication of SAFe-SBA *via* straightforward strategy. (b) HAADF-STEM image of SAFe-SBA and (c) corresponding element mapping. (d) AC-HAADF-STEM image of SAFe-SBA. (e) K-edge XANES spectra of SAFe-SBA. (f) FT k^3-weighted EXAFS of SAFe-SBA. Reproduced with permission [34]. Copyright 2019, American Chemical Society. (g) Wavelet transform of SAFe-SBA. Configurations models of SBA-15 and UNCu-SBA (h) top view and (i) side view. (j) HAADF-STEM image of UNCu-SBA. (k) AC-HAADF-STEM image of UNCu-SBA. Reproduced with permission [35]. Copyright 2020, American Chemical Society.

In fact, not only mesoporous silica, but various silicon-based minerals (such as diatomite, montmorillonite, kaolin, clay) can also be used as silicon-based materials for the preparation of SACs [32,41]. Diatomite is a kind of siliceous sedimentary rock with abundant reserves and low cost. Its chemical composition is mainly based on the SiO_2, and it has the characteristics of porosity, low density and high specific surface area. Dong *et al.* prepared diatomite-based Co-Si-N monatomic catalyst by metal enrichment/HF acid etching process (*p*-$CoSi_1N_3$@D) [32]. Firstly, cobalt acetate and dopamine hydrochloride were ultrasonic loaded onto diatomite, and then pre-annealed at 400 °C and 500 °C in the N_2 atmosphere for 2 h to obtain the Co-SAC structure containing diatomite shell structure (Fig. 4a). Co-Si SACs (*p*-$CoSi_1N_3$@D) with diatomite-like structure was finally obtained by etching the diatomite template in HF (20%) solution for 24 h (Figs. 4b-d). Because diatomite has a porous property similar to mesoporous silica, it can also be used to prepare single atom catalyst with silicon-based support without etching [41]. Tan *et al.* used the purified diatomaceous earth as a carrier to adjust the dispersion of ZiF-8 loaded with iron [41], and then calcined Fe-ZiF-8/diatomite powder under N_2 flow at 900 °C for 2 h to remove Zn atoms and obtain Fe-SACs/diatomite (Fig. 4e). The regular pore structure of diatomite endowed the excellent adsorption capacity for the loading of ZiF-8, so as the iron element of Fe-SACs could be well distributed in the diatomite carrier, which was also confirmed by its Energy dispersive spectrometer (EDS) mappings (Figs. 4f and g).

In addition to solid silicon-based materials (SiO_2, silicon-based minerals), some organosilicon sources can also be converted into silicon-based single atom catalysts doped with silicon structures [37]. Cao *et al.* disclosed an iron-doped metal-organic skeleton (MOF) precursor (ZnFe-ZIF-Si) that was initially prepared organically by the assembly of Zn^{2+} and Fe^{3+} with 2-methylimidazole, with an organosilicon source (tetraethyl orthosilicate) encapsulated in the precursor [37]. Subsequently, Fe-N-C-Si catalyst was obtained by high temperature of pyrolysis (Fig. 4h). The catalyst still has a typical MOF structure, and the single atom catalytic sites are evenly distributed on the MOF-derived carbon-based support (Figs. 4i and j). However, at present, there are few researches on the use of organosilicon sources or the preparation of SACs catalysts, and more organosilicon materials need to be developed in the future to realize the development of preparation strategies for silicon-based SACs.

Basically, a series of precursors for the preparation of silicon-based SACs encompass a diverse range of silicon-based substances, such as mesoporous silica, silicon-based minerals, and organosilicon materials. The preparation approaches involve the potential utilization of the channels of these silicon-based substances for the fixation of the single atomic structure (either with or without the silicon-based template, yet the majority of studies have etched the silicon-based template), and the possibility of employing silicon-based Si-OH and single atomic sites to construct novel metal-silicon configurations.

3. Basic performance and catalytic mechanism of silicon-based SACs

Since the channels of various silicon-based substances can be utilized for the fixation of the single atomic structure as space-

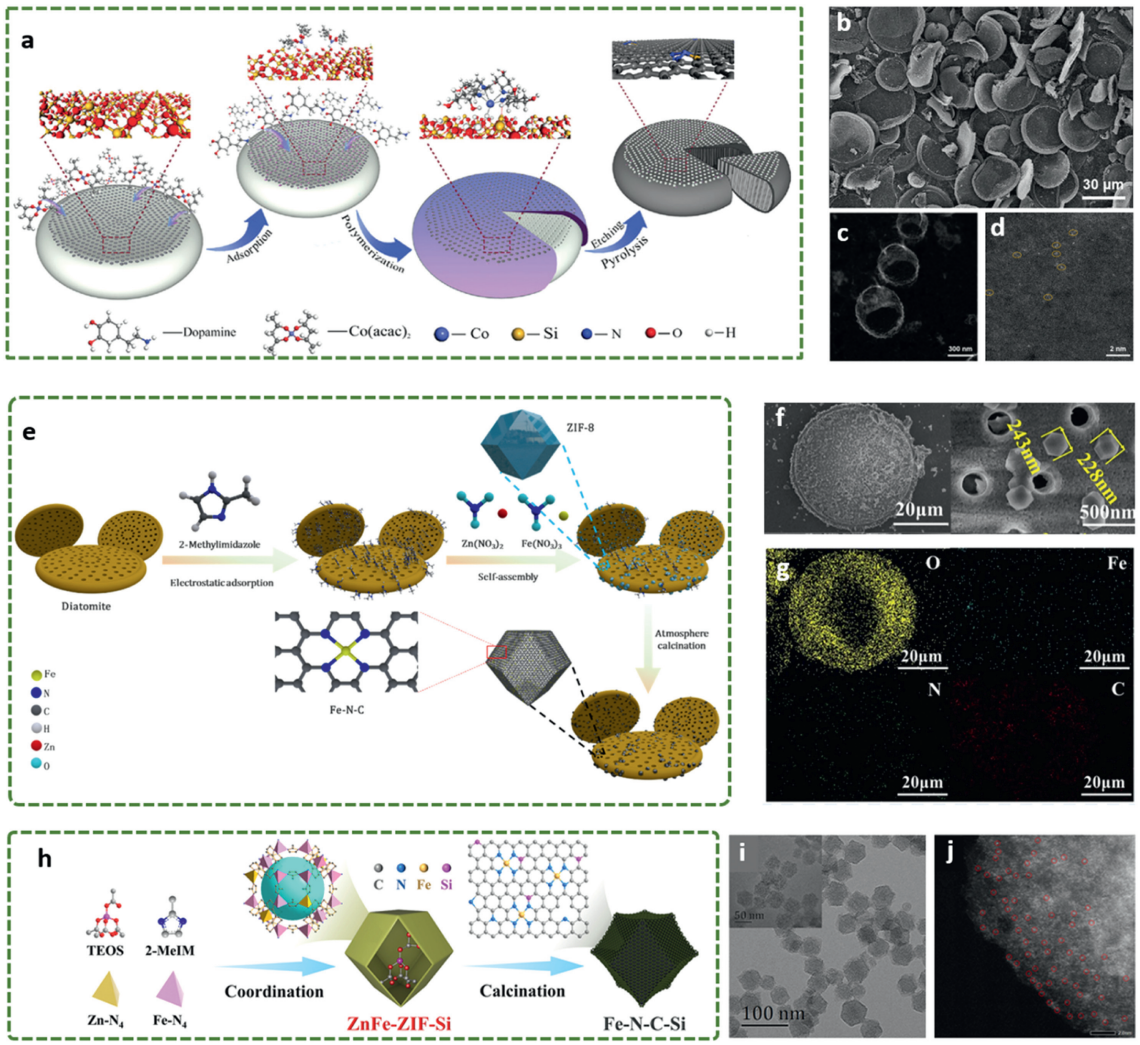

Fig. 4. (a) Schematic illustration of the synthesis procedure for p-$CoSi_1N_3$@D based on the diatomite. (b) SEM, (c) TEM, and (d) HAADF-STEM of the $CoSi_1N_3$@D. Reproduced with permission [32]. Copyright 2022, Wiley Ltd. (e) Scheme of F-SAC/diatomite. (f) SEM image and (g) EDS of the F-SAC/diatomite. Reproduced with permission [41]. Copyright 2019, Elsevier Inc. (h) Fabrication of Fe-N-C-Si using the organosilicon source. (i) TEM of the Fe-N-C-Si. (j) Aberration corrected (AC)-high-angle annular dark field (HAADF)-scanning transmission electron microscopy (STEM) image of Fe-N-C-Si. Reproduced with permission [37]. Copyright 2023, Exclusive Licensee Science and Technology Review Publishing House.

confined catalysts, or there is the possibility of employing silicon-based Si-OH and single atomic sites to construct novel metal-silicon configurations, the catalytic performances and mechanisms of silicon-based single-atom catalysts (SACs) would vary according to their fabrication strategies [27,28].

The fixation of single atomic sites in the nanoconfined space always would result in some nanoconfined effect towards the peroxide activation as well as pollutant degradation [27]. For example, Li *et al.* revealed a fundamental catalytic pathway transition of Co-SAC triggered by nanoconfinement using mesoporous silica as carrier [5]. They found that the CoNC-MSi1/peroxymonosulfate (PMS) system showed unprecedented high activity in selectively degrading electron-rich contaminants and demonstrated excellent stability, which was beneficial for water treatment applications (Figs. 5a and b). In addition, mesoporous silica confinement induced the electron transfer process (ETP) pathway, while the non-confined system was dominated by the $^1O_2$ mechanism (Fig. 5c). Thus, the ETP pathway may provide an opportunity to develop spatially decouple pollutant oxidation and oxidant activation processes (*i.e.*, no direct contact of oxidants with water contaminants is required) to facilitate aquatic environmental remediation, thereby avoiding the chemical waste and ecological risks of traditional advanced oxidation techniques. Of course, the nanoconfined strategy they mentioned can also be easily extended to other silicon-based SACs with similar structures. For instance, Wan and colleagues also reported a key role in the degradation of emerging pollutants in the hollow-nanoconfined effect, whereby the electronic structure of the active site can be adjusted to accelerate catalytic oxidation [42]. Additionally, the electronegativity of Si (1.90) is theoretically significantly lower than that of N (3.04), P (2.19), S (2.58), and B (2.04) [43]. Consequently, modulating single atom sites with Si heteroatoms proves to be a more efficacious strategy for reducing the energy barrier of PMS molecules to the active site [32]. Furthermore, Dong *et al.* reported that Si-heteroatomized p-$CoSi_1N_3$@D inherits the layered porous structure of diatomite, offering more accessible cobalt sites and open diffusion channels for PMS and contaminants in water treatment applications [32]. Based on the aforementioned concepts (optimal coordination structure and porous structure), p-$CoSi_1N_3$@D can serve as a highly active catalyst for PMS activation, with a turnover rate 2–3 orders of magnitude higher than those of transition metals SACs or oxides for bisphenol A (BPA) degradation in the published literature.

Besides PMS systems, Sun and colleagues discovered that silicon-based SACs using the SBA-15 as the carrier could likewise

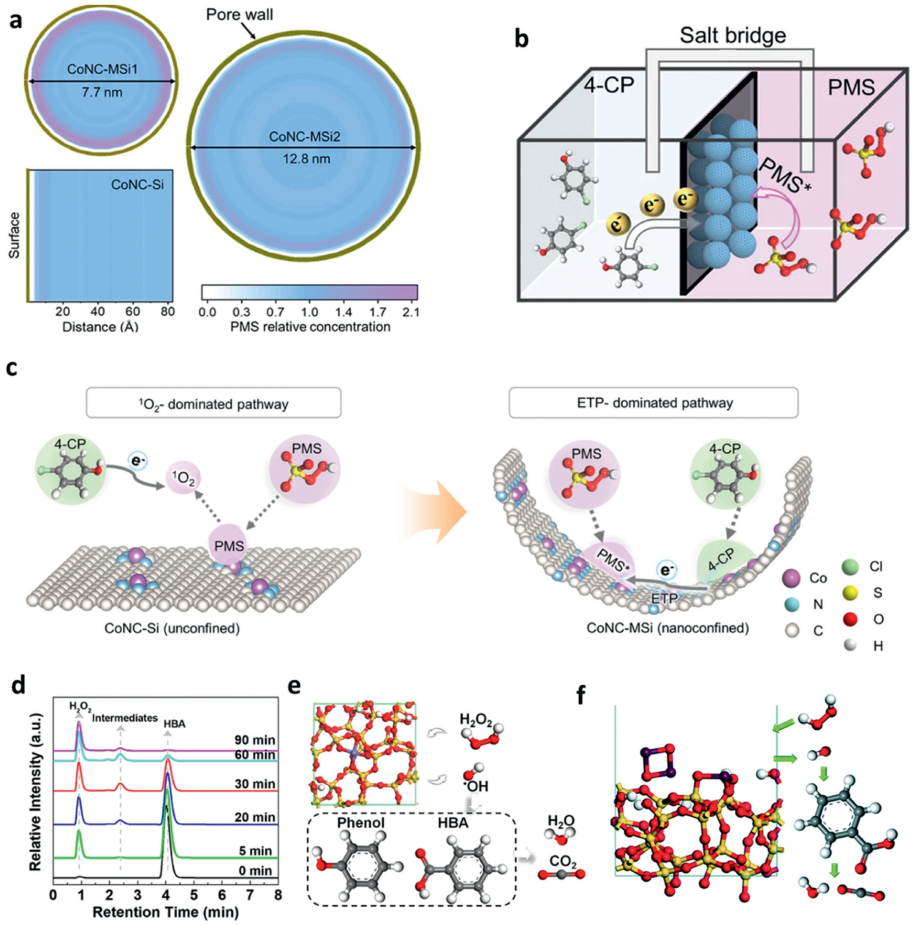

Fig. 5. (a) PMS concentration distributions obtained *via* the molecular dynamic simulations. (b) Scheme of ETP-based system for CoNC-MSi1/PMS system. (c) Mechanism difference between the mesoporous silica confinement and non-confined systems. Reproduced with permission [5]. Copyright 2024, The Nature Ltd. (d) HBA oxidation performance in SAFe-SBA/H_2O_2 system. (e) Mechanism scheme for H_2O_2 activation by SAFe-SBA. Reproduced with permission [34]. Copyright 2019, American Chemical Society. (f) Mechanism scheme for H_2O_2 activation by UNCu-SBA. Reproduced with permission [35]. Copyright 2020, American Chemical Society.

break the bottleneck related to the narrow pH conditions (pH 2–4) in H_2O_2 systems [21,34,35]. For instance, $Fe(NO_3)_3$ decomposed in a confined space of single-atom SAFe-SBA catalyst with a multitude of Si-OH groups, thereby ensuring the dispersion of the iron site at the atomic level within the nanopore [21,34]. Compared to the aggregation of iron sites, the SAFe-SBA catalyst exhibited stronger activity for the degradation of *p*-hydroxybenzoic acid (HBA) and phenol with high concentrations of radical at higher pH conditions (Figs. 5d and e) [34]. Ultrafine CuO nanoclusters and Cu single atoms were anchored onto the typical mesoporous silica SBA-15 (UNCu-SBA) for Fenton-like reactions [35]. The Cu mass normalized rate constant of UNCu-SBA is 18 times that of NPs, signifying that UNCu-SBA had exceptional Cu atomic utility (Fig. 5f). Specially, they reported that the UNCu-SBA catalyst could activate H_2O_2 to generate ·OH within a broader pH range of 4–7 compared to the typical Fenton reaction within the pH range of 2–4. These phenomena offer a novel approach for the silicon-based SACs to address the key bottlenecks that restrict traditional Fenton catalysis.

4. Density functional theory (DFT) analysis

DFT can also be effective for clarifying the activation mechanism of peroxide by various structures of silicon-based SACs. Based on the two basic structures of silicon-based SACs, such as (i) nanoconfined SACs in and (ii) SACs with metal-silicon configurations, DFT calculation can be used for the assessment of nanoconfinement and electronic properties of metal-silicon configurations [5,6,24,32,34,35,42].

Li and colleagues assessed the function of diverse structures regarding pathway alterations in silicon-based nanoconfinement based on DFT calculations [5]. They discovered that the transition from Co-N_3 to Co-N_4 marginally augmented the electron transfer quantity and PMS adsorption in unconstrained structures, indicating that N coordination numbers alone do not regulate the catalytic pathway [5]. It is notable that the escalation of N coordination number gives rise to more vacant 3D orbitals of Co under nanoconfinement, which verified that the valence state of Co ascended. Hence, nanoconfined Co SACs could furnish more PMS binding energy and interfacial charge transfer quantity than unconfined Co SACs, thereby facilitating the formation of PMS* (Figs. 6a-d). These outcomes disclosed that the ETP pathway of nanoconfined Co SACs was strengthened along with the increase in N coordination and emphasized the potential of other nanoconfined effects in redirecting catalytic pathways [42]. Wan and coworkers also reported the similar silicon-based nanoconfinement for electron-transfer enhancement [42]. Dong *et al.* deliberated the impact of Si substitution on PMS activation using the most energy-favorable structures (CoN_4 and $CoSi_1N_3$) [32]. They found that the positive charge distribution density at the center of the Co atoms in $CoSi_1N_3$ configuration was lower than that in the conventional CoN_4 configuration (Figs. 6e and h). They also reported that when PMS molecules were adsorbed at the Co atom center of CoN_4 and $CoSi_1N_3$ configurations, the $CoSi_1N_3$ moiety exhibited a greater

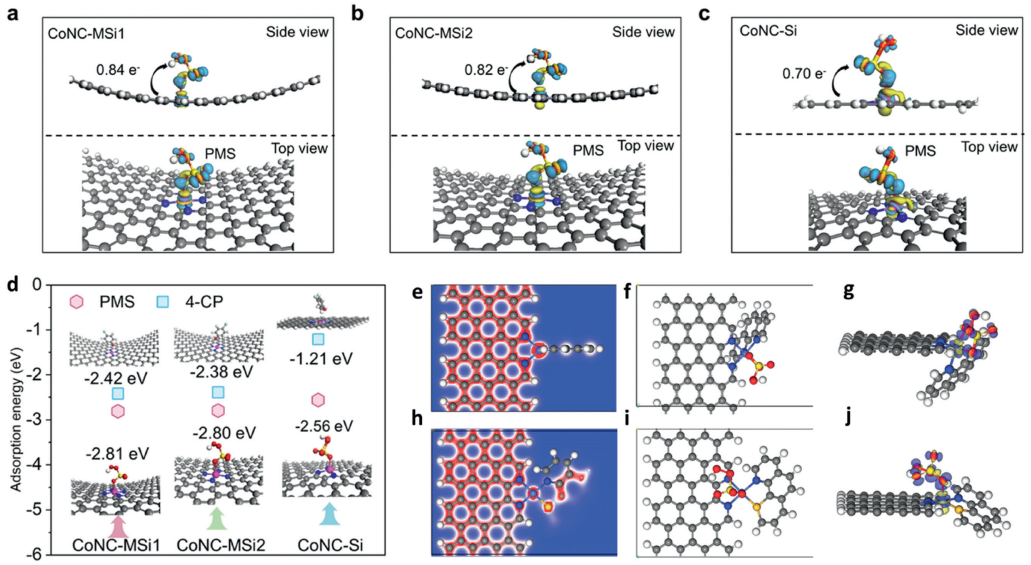

Fig. 6. (a-c) Adsorption configurations of PMS adsorption onto different SACs with/without nanoconfinement as well as their charge density differences. (d) Configurations and affinity of PMS/pollutants adsorption onto different SACs with/without nanoconfinement. Reproduced with permission [5]. Copyright 2024, The Nature Ltd. Differential charge densities of (e) CoN_4 and (h) $CoSi_1N_3$. The optimized adsorption structure of PMS molecules on (f) CoN_4 and (i) $CoSi_1N_3$. Differential charge densities of PMS adsorbed on the Co atoms for (g) CoN_4 and (j) $CoSi_1N_3$ configurations. Reproduced with permission [32]. Copyright 2022, Wiley Ltd.

electron density difference compared to CoN_4 (Figs. 6f-j). This phenomenon demonstrated that the electron transfer efficiency was significantly enhanced after doping Si atoms in the CoN_4 group, and the adsorption of PMS on $CoSi_1N_3$ was thermodynamically feasible. In contrast, the lower adsorption energy of $CoSi_1N_3$ implied that the Si and N bi-coordination of the single-atom Co site considerably expedites the interaction and electron transfer between PMS molecules and the atomic center. These discoveries revealed the significant role of Si doping in modulating the geometric and electronic structure of CoN_4 groups, thereby uncovering the reason for the enhanced catalytic performance of p-$CoSi_1N_3$@D for PMS activation [32].

However, in these simulations, the models of catalytic sites and the adsorption models for different peroxides are consistently overly optimized. Hence, for explaining the mechanism in these catalytic systems through DFT calculation, it is imperative to examine the catalytic configuration in multiple manners. Additionally, to depict or predict more precise catalytic processes, more intricate computational approaches need to be integrated. For instance, molecular dynamics can simulate the actual surface dynamic reaction process, set the number of molecules in accordance with the reaction conditions, and can be employed as a DFT method for studying catalytic processes. On the other hand, combining specific experimental studies with DFT calculations is also one of the crucial keys to clarifying the catalytic mechanism and rationalizing the observed reaction trends.

5. Conclusion and prospect

A series of precursors for the preparation of silicon-based SACs encompass a diverse range of silicon-based substances, such as mesoporous silica, silicon-based minerals, and organosilicon materials. The preparation approaches involve the potential utilization of the channels of these silicon-based substances for the fixation of the single atomic structure (either with or without the silicon-based template, yet the majority of studies have etched the silicon-based template), and the possibility of employing silicon-based Si-OH and single atomic sites to construct novel metal-silicon configurations. The SACs fabricated by the aforementioned two methods can conspicuously facilitate the activation of oxidants and promote the efficient degradation of pollutants, and exhibit superior stability compared to traditional carbon-based SACs. Nevertheless, the current research on silicon-based SACs still requires the resolution of the following issues in the future.

(i) The ultimate objective of preparing various silicon-based SACs is to implement them in practical and large-scale water treatment. Numerous preparation strategies are primarily based on the rational design of catalytic sites or catalyst structures. The intricate manufacturing process and high cost of these silicon-based SACs will impede their practical application. Therefore, in the long term, template preparation does not possess a green application prospect, and mineral resources have greater application potential.

(ii) In addition, the installation of silicon-based SACs constitutes the key to the application of these highly efficient catalysts in practical water treatment systems. In contrast to the complex design of various catalysts, the construction of catalyst devices can better enhance the applicability. The catalytic device can more effectively promote the decomposition of various peroxides and improve the utilization rate of free radical/non-free radical reaction substances. Currently, there are only sporadic studies on catalytic films in the research of silicon-based SACs; thus, it is necessary to intensify the systematic research of silicon-based SACs. The utilization of scale-up devices in subsequent large-scale trials also presents new challenges to the design and cost of these devices.

Declaration of competing interest

The authors declare that they have no known competing financial interests or personal relationships that could have appeared to influence the work reported in this paper.

CRediT authorship contribution statement

Hanghang Zhao: Writing – review & editing, Writing – original draft, Visualization, Supervision, Project administration. **Wenbo Qi:** Writing – original draft, Visualization, Conceptualization. **Xin Tan:** Software, Resources, Methodology, Conceptualization. **Xing Xu:**

Project administration, Investigation, Conceptualization. **Fengmin Song:** Investigation, Data curation. **Xianzhao Shao:** Project administration, Data curation, Conceptualization.

Acknowledgments

The research work was supported by National Natural Science Foundation of China (No. 52170086) and Natural Science Foundation of Shandong Province (No. ZR2021ME013), and Natural science Foundation of Shaanxi province (No. 2024JC-YBQN-0252), and Special Scientific Research Project of Hanzhong City-Shaanxi University of Technology Co-construction State Key Laboratory (No. SXJ-2106). The authors also want to thank Conghua Qi from Shiyanjia Lab (www.shiyanjia.com).

References

[1] X. Wu, J.H. Kim, ACS EST Engg. 2 (2022) 1776–1796.
[2] Q. Zeng, Y. Wen, X. Duan, et al., Appl. Catal. B: Environ. 346 (2024) 123752.
[3] Y. Shang, Y. Kan, X. Xu, Chin. Chem. Lett. 34 (2023) 108278.
[4] G. Yu, Y. Wu, H. Cao, et al., Environ. Sci. Technol. 56 (2022) 7853–7863.
[5] Y. Meng, Y.Q. Liu, et al., Nat. Commun. 15 (2024) 5314.
[6] J. Guo, Y. Wang, Y. Shang, et al., Proc. Natl. Acad. Sci. U. S. A. 121 (2024) e2313387121.
[7] Y. Gao, C. Yang, M. Zhou, et al., Small 16 (2020) 2005060.
[8] J. Jiang, S. Liu, D. Shi, et al., Water Res. 244 (2023) 120502.
[9] M.X. Gu, L.P. Gao, S.S. Peng, et al., ACS Nano 17 (2023) 5025–5032.
[10] H. Mai, T.C. Le, D. Chen, et al., Chem. Rev. 122 (2022) 13478–13515.
[11] Y. Shang, X. Xu, B. Gao, et al., Chem. Soc. Rev. 50 (2021) 5281–5322.
[12] X. Niu, W. Zheng, T. Song, et al., Chin. Chem. Lett. 34 (2023) 107560.
[13] Y. Zhang, S. Liu, D. Chen, et al., Chin. Chem. Lett. 35 (2024) 108666.
[14] C.H. Gu, Y. Pan, T.T. Wei, et al., Nat. Water 2 (2024) 649–662.
[15] Y.J. Zhang, J.S. Tao, Y. Hu, et al., Nat. Water 2 (2024) 770–781.
[16] M. Mainardis, C. Ferrara, B. Cantoni, et al., Sci. Total Environ. 906 (2024) 167598.
[17] G. Cai, T. Liu, J. Zhang, et al., Water Res. 219 (2022) 118540.
[18] X. Chen, W. Fu, Z. Yang, et al., Water Res. 230 (2023) 119562.
[19] X. Cheng, H. Guo, Y. Zhang, et al., Water Res. 157 (2019) 406–414.
[20] Y.H. Chuang, A. Szczuka, F. Shabani, et al., Water Res. 152 (2019) 215–225.
[21] Y. Gao, Y. Luo, Z. Pan, Z. Zeng, et al., Water Res. 249 (2024) 120967.
[22] Y. Gao, P. Wang, Y. Chu, et al., Water Res. 248 (2024) 120826.
[23] F. Gosselin, L.M. Madeira, T. Juhna, et al., Water Res. 47 (2013) 5631–5638.
[24] J. Guo, B. Gao, Q. Li, et al., Adv. Mater. 36 (2024) 2403965.
[25] J. Song, N. Hou, X. Liu, et al., Adv. Mater. 35 (2023) 2209552.
[26] Z. Zhao, H. Tan, P. Zhang, et al., Angew. Chem. Int. Ed. 62 (2023) e202219178.
[27] Y. Yao, C. Wang, X. Yan, et al., Environ. Sci. Technol. 56 (2022) 8833–8843.
[28] X. Pan, S. Mei, W.J. Liu, Chin. Chem. Lett. 34 (2023) 108034.
[29] K. Yin, J. Yang, Y. Li, et al., Chin. Chem. Lett. 35 (2024) 109847.
[30] Y. Zhang, S. Liu, D. Chen, et al., Chin. Chem. Lett. 35 (2024) 108666.
[31] Z.Y. Guo, R. Sun, Z. Huang, et al., Proc. Natl. Acad. Sci. U. S. A. 120 (2023) e2220608120.
[32] X. Dong, Z. Chen, A. Tang, et al., Adv. Funct. Mater. 32 (2022) 2111565.
[33] M.K. Sarangi, L.D. Patel, G. Rath, et al., Chin. Chem. Lett. 35 (2024) 109381.
[34] Y. Yin, L. Shi, W. Li, et al., Environ. Sci. Technol. 53 (2019) 11391–11400.
[35] Y. Yin, W. Li, C. Xu, et al., Environ. Sci: Nano. 7 (2020) 2595–2606.
[36] J. Lin, L. Jiang, W. Tian, et al., J. Mater. Chem. A 11 (2023) 13653–13664.
[37] C. Cao, S. Zhou, S. Zuo, et al., Research 6 (2023) 0079.
[38] Y. Berro, S. Gueddida, Y. Bouizi, et al., J. Colloid Interface Sci. 573 (2020) 193–203.
[39] L. Jiao, R. Zhang, G. Wan, et al., Nat. Commun. 11 (2020) 2831.
[40] X. Bai, Y. Guo, Z. Zhao, Chin. Chem. Lett. 33 (2022) 1325–1330.
[41] Y. Tan, S. Yang, C. Li, et al., Surf. Interfaces 48 (2024) 104352.
[42] M. Tang, J. Wan, Y. Wang, et al., Water Res. 249 (2024) 120950.
[43] K. Yin, W. Hong, J. Yang, et al., Environ. Pollut. 348 (2024) 123825.